Journal of Power Sources 196 (2011) 2810–2818

Contents lists available at ScienceDirect

Journal of Power Sources

journal homepage: www.elsevier.com/locate/jpowsour

A polyethylene glycol-assisted carbothermal reduction method to synthesize $LiFePO_4$ using industrial raw materials

George Ting-Kuo Fey[a,*], Kai-Pin Huang[a], Hsien-Ming Kao[b], Wen-Hsien Li[c]

[a] Department of Chemical and Materials Engineering, National Central University, Chung-Li 32054, Taiwan
[b] Department of Chemistry, National Central University, Chung-Li 32054, Taiwan
[c] Department of Physics, National Central University, Chung-Li 32054, Taiwan

ARTICLE INFO

Article history:
Received 19 July 2010
Received in revised form 6 November 2010
Accepted 9 November 2010
Available online 16 November 2010

Keywords:
Lithium iron phosphate cathode
Carbothermal reduction method
Industrial raw material
Polyethylene glycol
Lithium-ion battery

ABSTRACT

Olivine $LiFePO_4$ is synthesized by a carbothermal reduction method (CTR) using industrial raw materials with polyethylene glycol (PEG) as a reductive agent and carbon source. A required amount of acetone is added to the starting materials for the ball milling process and the precursor is sintered at 973 K for 8 h to form crystalline phase $LiFePO_4$. The structure and morphology of the $LiFePO_4$/C composite samples have been characterized by X-ray diffraction, field-emission scanning electron microscopy, transmission electron microscopy, energy-dispersive spectroscopy, differential scanning calorimetry and magnetic susceptibility. Electrochemical measurements show that the $LiFePO_4$/C composite cathode delivers an initial discharge capacity of 150 mAh g^{-1} at a 0.2*C*-rate between 4.0 and 2.8 V, and almost no capacity loss is observed for up to 50 cycles. Remarkably, the cell can sustain a 30*C*-rate between 4.6 and 2.0 V, and this rate capability is equivalent to charge or discharge in 2 min. The simple technique, low-cost starting materials, and excellent electrochemical performance make this process easier to commercialize than other synthesized methods.

1. Introduction

Olivine-structured lithium iron phosphate ($LiFePO_4$) proposed by Goodenough et al. is a popular cathode material because of its low toxicity, remarkable thermal stability, low raw materials' cost, and a relatively high theoretical specific capacity of 170 mAh g^{-1} with a discharge voltage plateau of 3.5 V versus Li/Li^+ [1–3]. However, the main obstacles that inhibit its use in large batteries for applications, such as HEVs, are poor electronic conductivity [1], slow lithium-ion diffusion [1], low tap density [4] and poor batch reproducibility [5]. To overcome the above problems, various methods have been widely used, such as lattice metal doping [6–9], particle-size optimizing [10,11], and conductivity layer coating with carbon [12–14], silver [15], copper [15], or lithium phosphate [16].

Unfortunately, the above methods are expensive because they either involve complicated steps or using expensive divalent iron compounds, such as $FeC_2O_4{\cdot}H_2O$, as the starting material. Barker et al. [17] first synthesized $LiFePO_4$/C by a carbothermal reduction (CTR) reaction using Fe_2O_3 as the starting material. CTR is simpler than a traditional solid-state reaction because it does not need pre-sintering treatment, preparation of intermediates, or other complicated synthesis techniques.

In recent years, various polymers have been used as carbon sources or additives for $LiFePO_4$/C composites, such as polystyrene (PS) [18], polypropylene (PP) [5], polyvinyl alcohol (PVA) [19], polypyrrole (PPy) [20], polyaniline (PANI) [21], polyethylene glycol (PEG) [22], and polyacene (PAS) [23]. Among these polymers, PEG has been widely used for many biomedical and electrochemical applications due to its immunogenicity, hydrophilicity, antigenicity, non-toxicity, and solubility in water and organic solvents [24]. Tajimi et al. reported a polyethylene glycol-assisted hydrothermal method to synthesize uniform $LiFePO_4$ particles [25]. Furthermore, Xu et al. [26] and Wang et al. [22] also used PEG-assisted sol–gel and rheological phase methods to synthesize $LiFePO_4$/C composites, respectively. They found that the presence of PEG during the synthesis process can control the morphology and size of the powders. The above mentioned syntheses of $LiFePO_4$/C employed a hydrothermal method, sol–gel method, and rheological phase method. The hydrothermal method requires expensive equipment to withstand high pressure. In the sol–gel method, starting materials are expensive and some additives might be required to control the pH value or chelate complexes into gels, which would increase both the cost and the complexity of synthesis. The rheological phase method needs crystalline hydrates, such as $FePO_4{\cdot}4H_2O$, as starting materials, which are not easy to store. In order to simplify the process, we used a PEG-assisted carbothermal reduction method

* Corresponding author. Tel.: +886 3 425 7325/422 7151x34206; fax: +886 3 425 7325.
E-mail address: gfey@cc.ncu.edu.tw (G.T.-K. Fey).

0378-7753/$ – see front matter © 2010 Elsevier B.V. All rights reserved.
doi:10.1016/j.jpowsour.2010.11.057

Table 1
The prices of industrial raw materials of iron salts, lithium salts, and phosphorus compounds in Taiwan.

	Company	Purity	US$ kg^{-1}	US$ kg^{-1} of one atom of Fe, Li, or P
Iron salts				
Fe_2O_3	Taiwan Polychem Co. Ltd.	T.G., 99 wt.%	2.125	1.063
$FeC_2O_4{\cdot}2H_2O$	Huacheng Industrial Co. Ltd.	T.G., 99 wt.%	8.750	8.750
$FeSO_4{\cdot}7H_2O$	First Chemical Works Co. Ltd.	T.G., 98 wt.%	1.563	1.563
Lithium salts				
Li_2CO_3	First Chemical Works Co. Ltd.	T.G., 99 wt.%	18.266	9.133
LiOH	First Chemical Works Co. Ltd.	T.G., 99 wt.%	21.875	21.875
Phosphorus compounds				
$NH_4H_2PO_4$	First Chemical Works Co. Ltd.	T.G., 99 wt.%	3.018	3.018
H_3PO_4	First Chemical Works Co. Ltd.	T.G., 85 wt.%	3.100	3.100
P_2O_5	First Chemical Works Co. Ltd.	T.G., 95 wt.%	37.500	18.750

to synthesize $LiFePO_4$/C, which could overcome the disadvantages of the above methods, because PEG is inexpensive, able to form a carbon network and easy to store. However, most importantly, it has high reduction ability.

In this paper, we have successfully used a simple and low-cost carbothermal reduction method to synthesize $LiFePO_4$/C composites with a good carbon network by using PEG as a carbon source and reducing agent and choosing industrial raw materials of ferric oxide, ammonium dihydrogen phosphate, and lithium carbonate as starting materials. The prices of these materials used in our studies are less expensive compared to other similar materials, as listed in Table 1. Through our work, we have significantly reduced the synthesis cost, simplified the synthesis process, and improved the cell performance of $LiFePO_4$/C composites.

2. Experimental

$LiFePO_4$/C composites were prepared by a CTR reaction involving a mixture of ferric oxide (T.G., 99 wt.%, Taiwan Polychem Co. Ltd.), ammonium dihydrogen phosphate (T.G., 99 wt.%, First Chemical Works Co. Ltd.), lithium carbonate (T.G., 99 wt.%, First Chemical Works Co. Ltd.) and reduction agent polyethylene glycol (T.G., M.W. = 6000, Huacheng Industrial Co. Ltd.) in a stoichiometric molar ratio. The precursor was mixed by ball-milling in the required amount of acetone for 2 h and the resulting gel was dried at 353 K in a furnace and thoroughly reground. Finally, the dried mixture was transferred to a temperature controlled tube furnace equipped with flowing N_2 gas and heated at 573 K for 2 h, then sintered at 973 K for 8 h. To coat $LiFePO_4$ with carbon, 80 wt.% PEG was used. The wt.% value of PEG was defined as the ratio of the weight of PEG to the weight of $LiFePO_4$.

Crystal structural analysis of the solid-state synthesized materials was carried out by X-ray diffraction (Siemens D-5000, Mac Science MXP18). The diffraction patterns were recorded between scattering angles of 15° and 80° in steps of 0.05°. Surface composition analysis was obtained by Raman spectroscopy (ISA T64000) and total organic carbon (TOC) instrument (OIA, Model Solids-TOC). Raman spectroscopy measurements were carried out at room temperature in ambient atmosphere. The power of the laser beam was adjusted to 50 mW, and the average acquisition time for each spectrum was 5 min. TOC was used to examine the carbon contents of $LiFePO_4$/C. The morphology of $LiFePO_4$/C composites was observed by scanning electron microscope (SEM; Hitachi S-3500V) and high-resolution transmission electron microscope (HR-TEM; Jeol TEM-2000FXII). The carbon distribution was confirmed with energy dispersive spectroscopy (EDS) (or energy dispersive X-ray spectrometry).

Coin cells of the 2032 configuration were assembled in an argon filled glove box (VAC MO40-1) in which the oxygen and water contents were maintained below 2 ppm. Lithium metal (Foote Mineral) was used as the anode and a 1 M solution of $LiPF_6$ in EC:DEC (1:1, v/v) (Tomiyama Chemicals) was used as the electrolyte. The cathode was prepared by mixing 85 wt.% $LiFePO_4$-based powders with 10 wt.% carbon black and 5 wt.% poly(vinylidene fluoride) (PVDF) in N-methyl-2-pyrrolidone (NMP) solution. The mixture was pasted on an aluminum foil and dried overnight at 393 K in an oven. The dried coated foil was roller-pressed and circular discs were punched out.

The coin cells were cycled at a 0.2*C*-rate (with respect to a theoretical capacity of 170 mAh g^{-1}) and 298 ± 0.5 K between 2.8 and 4.0 V in a Maccor 4000 multi-channel battery tester. All electrochemical experiments were conducted at room temperature in a glove-box filled with high purity argon. The conductivity measurements were performed using a four-point d.c. probe (Keithly 2400, SR-4 four-point probe).

Phase transitions occurring during the cycling processes were examined by a cyclic voltammetric experiment, performed with a three-electrode glass cell. The working electrode was prepared with the cathode powders, as described above, but coated on both sides of the aluminum foil. The cell for the cyclic voltammetric studies was assembled inside a glove box with lithium metal foil serving as both counter and reference electrodes. The electrolyte used was the same as that for the coin cell. Cyclic voltammograms were run on a Solartron 1287 Electrochemical Interface at a scan rate of 0.1 mV s^{-1} between 2.7 and 4.5 V.

A Sieko SSC 5000 TG/DTA equipment was used for thermal analysis. The analysis was done in argon between room temperature and 1173 K at a heating ramp of 10 K min^{-1} with a 50 mg sample. Thermal stability analysis was carried out on a Perkin Elmer DSC 7 differential scanning calorimetry (DSC) for pristine $LiFePO_4$ and carbon-coated $LiFePO_4$. The measurements were performed in nitrogen atmosphere between 303 and 673 K, at a heating rate of 10 K min^{-1}. The samples for the DSC experiments were prepared as follows. The coin cells were first galvanostatically charged to 4.5 V at a 0.2*C*-rate and then potentiostated at 4.5 V for 10 h. The coin cells were then opened inside a glove box. The cathode in the coin cell was carefully removed, and the excess electrolyte was wiped with Kimwipes. The cathode was gently scraped from the aluminum current collector, loaded on to an aluminum pan, hermetically sealed, placed in an airtight container, and transferred to the DSC instrument.

The magnetic susceptibility experiments were carried with a Quantum Design PPMS magnetometer at a field of 1 Oe.

3. Results and discussion

3.1. Thermal analysis

In order to determine the decomposition and crystallization temperatures of the CTR-precursor, we adopted TGA and DTA

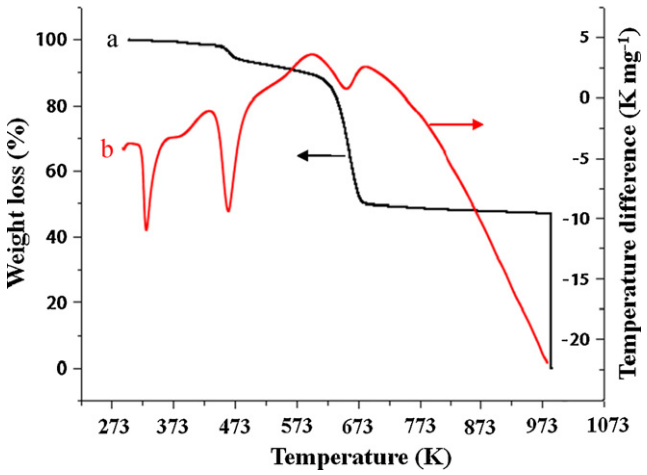

Fig. 1. TGA/DTA curves of the CTR-precursor with 80 wt.% PEG: (a) TGA curve and (b) DTA curve.

analyses prior to the optimization of the synthesis process. Fig. 1 shows the TGA/DTA curves of the CTR-precursor with 80 wt.% PEG obtained after ball-milling, while Fig. 2 displays the TGA curve of the PEG reducing agent. There was a three-stage weight loss process in Fig. 1, with the first-stage below 473 K due to the loss of superficial moisture from the precursor. A strong exothermic peak appeared near 327 K, which was caused by the phase change of PEG from solid to liquid. The second stage with a strong exothermic peak near 473 K occurred from 473 to 623 K, which could be attributed to the decomposition of $NH_4H_2PO_4$. The third stage that occurred from 623 to 673 K was mainly related to the decomposition of PEG, as confirmed in Fig. 2. The weight loss of the precursor in the third stage was about 38 wt.% because it decomposed to form C, CO, CO_2 and H_2O [27]. There was a slight weight loss at above 673 K, related to the reaction of carbon with residue oxygen and the crystallization process of olivine $LiFePO_4$. The continuously exothermic curve that occurred at above 683 K in the DTA analysis under flowing nitrogen was due to the crystallization process of $LiFePO_4$ [28]. We conclude that the crystallization of CTR-$LiFePO_4$/C composites can be confirmed at about 700 K, but it is known from the results reported in other papers [17,29–31] that the best temperature to produce crystalline CTR-$LiFePO_4$ samples is 923–1023 K. Based on the above analyses, we preheated the CTR-precursor at 573 K for the decomposition of $NH_4H_2PO_4$ and then calcined at 973 K for the crystallization of $LiFePO_4$.

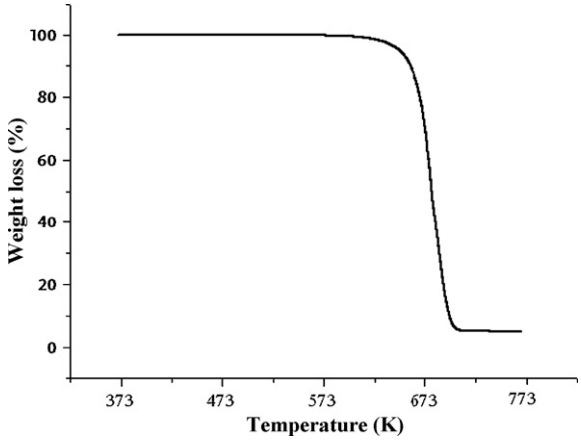

Fig. 2. TGA curve of the PEG.

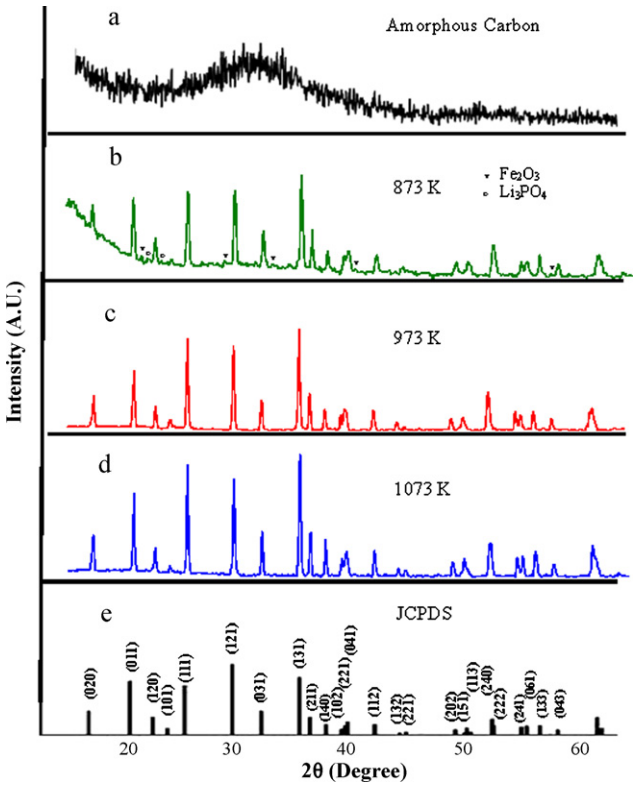

Fig. 3. XRD patterns of (a) amorphous carbon; the CTR-$LiFePO_4$/C composites synthesized at (b) 873 K; (c) 973 K; (d) 1073 K; (e) JCPDS card no. 40-1499 of $LiFePO_4$.

3.2. X-ray diffraction

The crystal structure and purity of the CTR-$LiFePO_4$/C composites, which were produced by using industrial raw materials, were studied by XRD analysis. The XRD patterns of CTR-$LiFePO_4$/C composites synthesized with 80 wt.% PEG at 873–1073 K are shown in Fig. 3. The sample prepared at 873 K mainly consisted of $LiFePO_4$ with minor Fe_2O_3 and Li_3PO_4 peaks. No impurities were detected at 973 K and 1073 K, as also confirmed by a magnetic susceptibility study that will be discussed later. The diffraction lines are indexed to the orthorhombic Pnma space group (JCPDS card no. 40-1499). These results imply that single phase $LiFePO_4$/C composites were successfully produced at 973 K and 1073 K using technical grade raw materials, indicating that PEG is an effective reducing agent for the reduction of Fe_2O_3.

The peaks of XRD patterns become sharper when temperature increases due to the highly crystalline structure [32]. The crystallite size (D) was calculated from the Scherrer equation $\beta\cos(\theta) = k\lambda/D$, where β is the full-width-at-half-maximum (FWHM) of the XRD peak (0 2 0) and k is a constant (0.91) [33,34]. From Scherrer's formula, the grain sizes of $LiFePO_4$/C synthesized at 873 K, 973 K, and 1073 K are 41.2, 48.1, and 50.8 nm, respectively. The above calculation shows that higher sintering temperature results in larger grain size, which is consistent with Kim et al.'s report [35], and the large grain size decreases the surface area of the materials and the Li^+ diffusion coefficient [36].

Fig. 3a shows a typical XRD pattern for amorphous carbon that generally displays a noisy background. The pattern of the CTR-$LiFePO_4$/C composite synthesized at 873 K (Fig. 3b) below 20° showed an upturned tail due to the existence of amorphous carbon, as confirmed in Fig. 3a [37]. The upturned tail was not found in the patterns of the $LiFePO_4$/C composites synthesized at 973 K and 1073 K due to a low ratio of amorphous carbon.

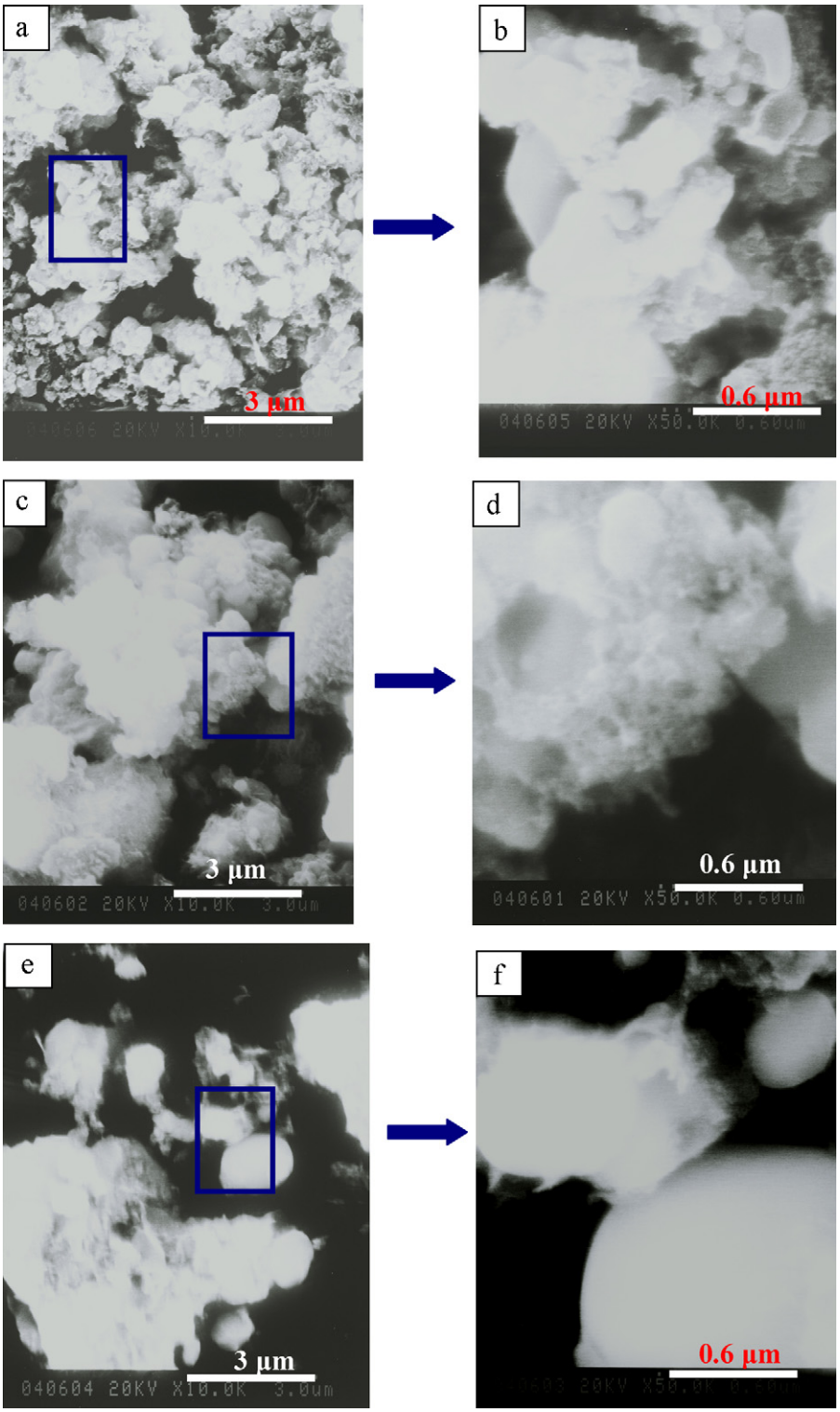

Fig. 4. SEM images of the CTR-$LiFePO_4$/C composites synthesized at (a) and (b) 873 K; (c) and (d) 973 K; (e) and (f) 1073 K; (b), (d), and (f) are partial enlargements of (a), (c), and (e), respectively.

3.3. Morphology

The morphological features of the CTR-$LiFePO_4$/C composite synthesized with 80 wt.% PEG were investigated by SEM and TEM. Fig. 4a, c and e shows the SEM images of the CTR-$LiFePO_4$/C composites synthesized at 873 K, 973 K, and 1073 K, respectively, and Fig. 4b, d, and f are partial enlargements corresponding to Fig. 4a, c, and e. The sample synthesized at 1073 K showed serious agglomeration and a particle size exceeding 3.0 μm. The samples synthesized at 873 K and 973 K exhibited smaller and more uniform particle size distribution of about 0.5–0.9 μm and 1.5–2.0 μm, respectively. The results clearly show that higher sintering temperature leads to larger average particle sizes, which is consistent with the XRD analysis. Small particle size allows easy penetration of the electrolyte and provides a short pathway for Li^+ diffusion in the active material crystals [9]. However, these values of particle size are quite

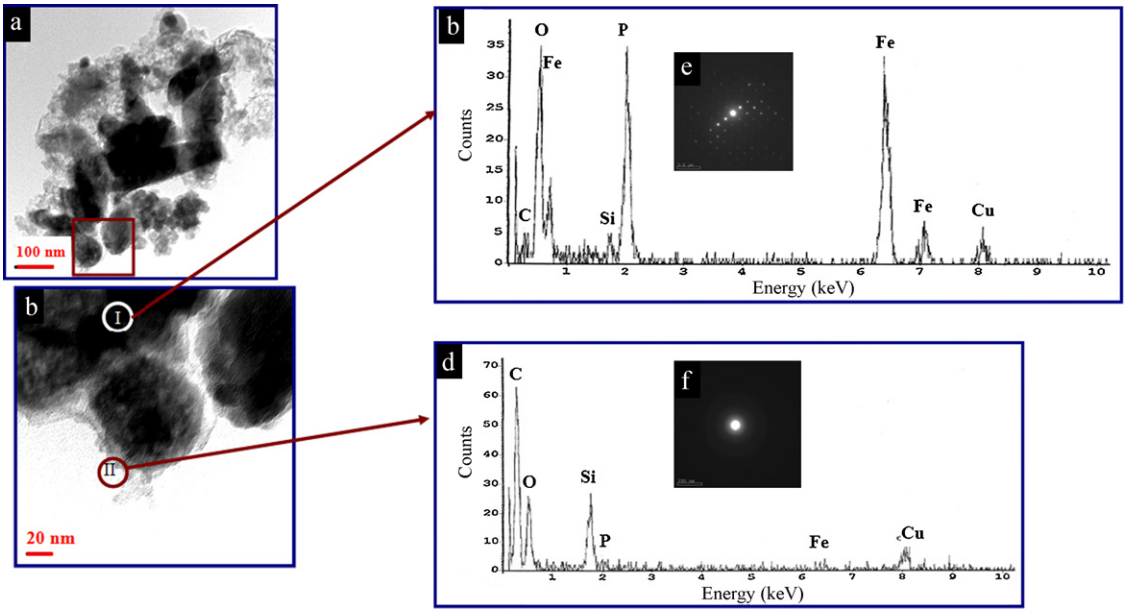

Fig. 5. TEM/SAED/EDS images of the CTR-$LiFePO_4$/C composite: (a) and (b) TEM images; (c) and (d) EDS analyses; (e) and (f) SAED patterns.

a bit larger than those calculated by Scherrer's formula, indicating the primary particles agglomerated to secondary particles. Yamada et al. reported an obvious growth in particle size when the sintering temperature rose above 873 K [38], which is similar to what happened in our study.

In order to analyze the morphology of CTR-$LiFePO_4$/C particles and the carbon coating layer on the particle surface in detail, TEM/SAED/EDS analyses were carried out. Fig. 5 shows the TEM/SAED/EDS images of the CTR-$LiFePO_4$/C composite synthesized at 973 K using 80 wt.% PEG as a carbon source. In Fig. 5e, the corresponding SAED pattern of region I showed a distinct lattice image, indicating a well-crystallized structure. Confirmed by EDS analysis (Fig. 5c), the peaks of Fe, P, and O are very clear in region I, which shows that the sample in region I might be well-crystallized $LiFePO_4$. In Fig. 5d and f, the corresponding EDS analysis and SAED pattern of region II showed a clear peak of carbon and only halo rings, respectively, which confirmed the presence of amorphous carbon. The TEM images in Fig. 5a and b show that there were distinct particles about 50–60 nm. These particles agglomerated to form secondary particles around 100–500 nm and were connected to the well-networked carbon, which might be carbonized from PEG, and this carbon network could substantially enhance the electronic conductivity to 4.42×10^{-4} S cm^{-1}. Based on the above results, from Scherrer's formula, SEM images, and TEM images, we conclude that CTR-$LiFePO_4$ crystal grains were about 50–60 nm, and aggregated to form 500 nm to ~2.0 μm secondary particles due to the aggregation of several carbon networks and $LiFePO_4$ particles.

3.4. Thermal stability

Olivine-structured lithium iron phosphate has remarkable thermal stability due to strong P–O bonds, which could tightly bind oxygen [39]. However, Yoon et al. showed that P–O bonds become less covalent during delithiation [40] and Delacourt et al. reported that Li-poor Li_xFePO_4 might transform into non-olivine phases at high temperature [41]. In order to study the thermal stability of the CTR-$LiFePO_4$/C composite under a delithiation condition, DSC analysis was carried out. Fig. 6 shows the DSC profiles of 4.5 V charged commercial $LiCoO_2$ and in-house CTR-$LiFePO_4$/C composites synthesized at 973 K with 80 wt.% PEG. After a series of charge and

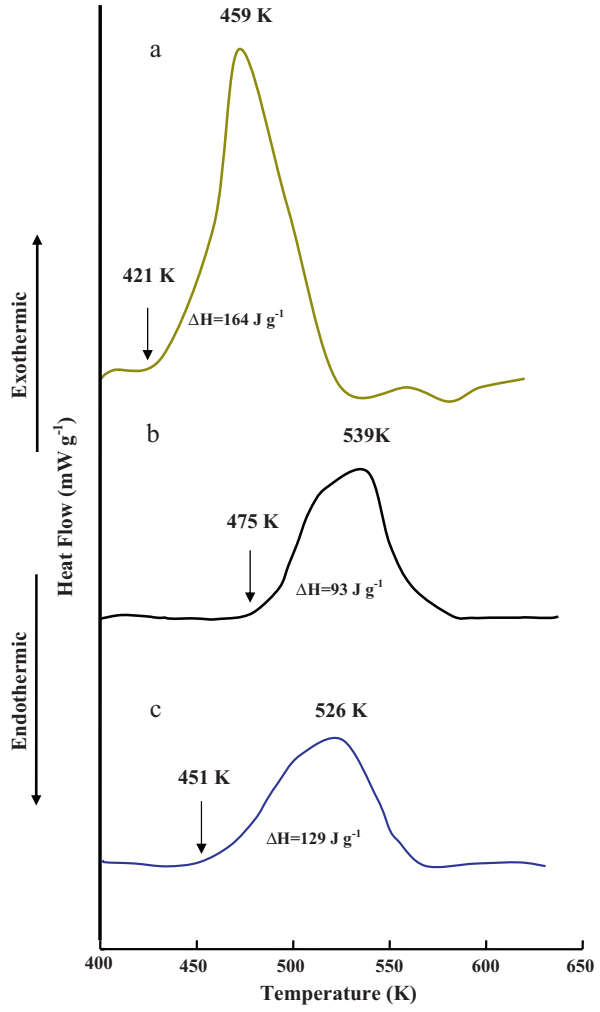

Fig. 6. DSC profiles of (a) commercial $LiCoO_2$; (b) the CTR-$LiFePO_4$/C; (c) the CTR-$LiFePO_4$/C (C.R. = 80%). Charged to 4.5 V.

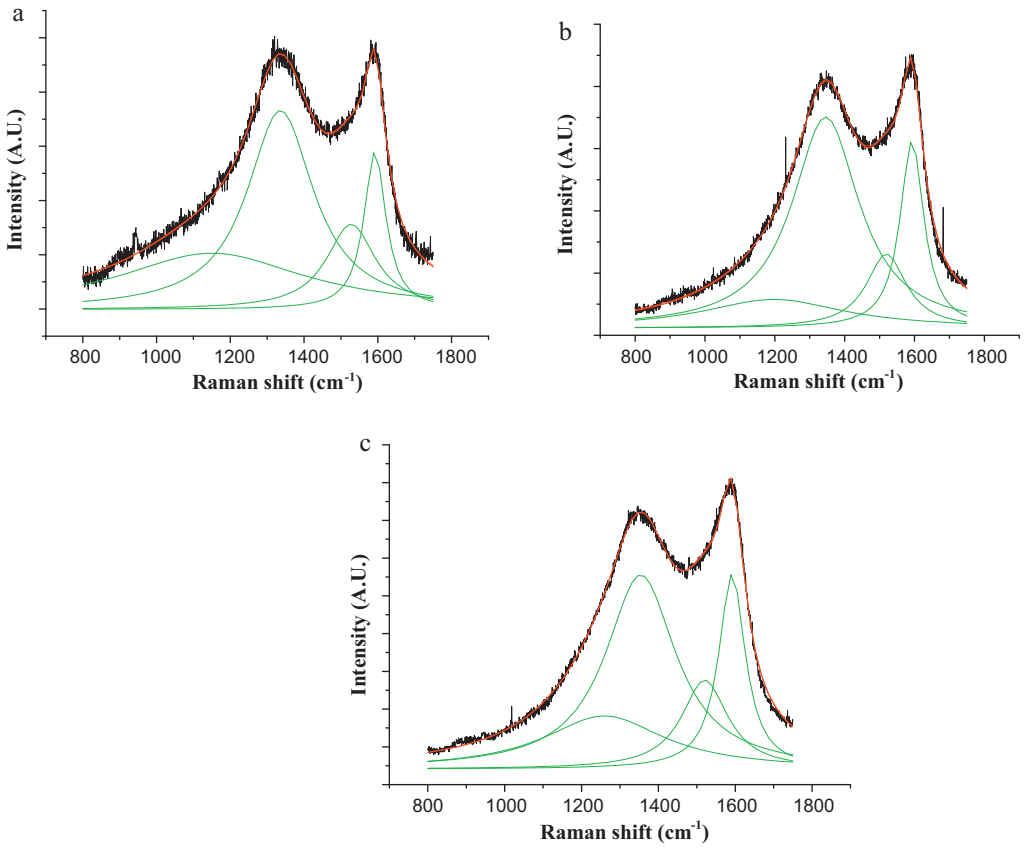

Fig. 7. Raman spectra of the CTR-$LiFePO_4$/C composites synthesized at (a) 873 K; (b) 973 K; (c) 1073 K.

discharge processes of $LiFePO_4$/C composites, we continued the DSC again when the cycle retention (C.R.) was equal to 80%, as shown in Fig. 6c. All exothermic heat flow was detected within a wide temperature range of 400–640 K. The total heat evolution of the $LiCoO_2$ material was 164 J g^{-1}, while the total heat evolution of the $LiFePO_4$/C and $LiFePO_4$/C (C.R. = 80%) materials was 92 and 129 J g^{-1}, respectively. From these thermal data, it is clear that the exothermic heat flow of the CTR-$LiFePO_4$/C composite is much smaller for the commercial $LiCoO_2$. The onset temperature of the $LiCoO_2$, $LiFePO_4$/C, and $LiFePO_4$/C (C.R. = 80%) samples are 421, 475, and 451 K. Therefore, it appears that commercial $LiCoO_2$ material has greater heat evolution and lower onset temperature because of significant oxygen loss [42]. The excellent thermal stability of the CTR-$LiFePO_4$/C composite could make it commercially feasible for large battery applications, such as EVs.

3.5. Raman spectra

Raman spectroscopy is a particularly useful tool for characterizing the structure of carbon. Fig. 7a–c is the typical Raman spectra of the CTR-$LiFePO_4$/C composites using 80 wt.% PEG as a carbon source synthesized at different sintering temperatures. All Raman spectra show two intense and broad bands located at ~1350 and ~1590 cm^{-1}, respectively. Doeff et al. [43,44] reported that the two broad bands can actually be deconvoluted into four peaks at around 1190, 1350, 1518, and 1590 cm^{-1}. The peaks at ~1190 and ~1518 cm^{-1} can be assigned to the sp^3-type carbon, and the ones at ~1350 and ~1590 cm^{-1} can be assigned to the D (disordered) and G (graphene) bands of sp^2-type carbon. A lower intensity ratio of the D/G band (I_D/I_G ratio) in Raman spectrum indicates more graphene clusters in the structure of carbon, which would enhance the electronic conductivity of the residual carbon.

In order to resolve the Raman spectra, a peak deconvolution procedure was used. There are two characteristic parameters, I_D/I_G and A_{sp^3}/A_{sp^2} ratios, obtained from the fitting procedure. The I_D/I_G ratio is obtained by dividing the area of D band and G band, while the A_{sp^3}/A_{sp^2} ratio is obtained by dividing the area of sp^3 carbon bands (~1190 and ~1518) and sp^2 G band (~1350 and ~1590 cm^{-1}). The I_D/I_G ratios of the CTR-$LiFePO_4$/C composites synthesized at 873 K, 973 K and 1073 K are 3.87, 2.94, and 2.65, respectively, while the A_{sp^3}/A_{sp^2} ratios are 0.88, 0.50, and 0.46, respectively, and the electronic conductivities of these samples are 3.44×10^{-5}, 4.42×10^{-4}, and 9.14×10^{-5} S cm^{-1}, respectively, as shown in Table 2. Higher sintering temperature clearly resulted in lower I_D/I_G and A_{sp^3}/A_{sp^2} ratios, indicating that more useful graphitized carbon became coated on the $LiFePO_4$ at 1073 K during the pyrolysis step. However, the electronic conductivity of the sample synthesized at 973 K is higher than the one synthesized at 1073 K. Electronic conductivity is not proportional to the ratio of conductive carbon coating, probably because it is affected by more factors than just the I_D/I_G ratio. Based on our previous results, morphology of carbon coating [14], the particle size of the active material [11], the thickness of the carbon coating layer [45], the kind of conductive carbon network [46], and the surface area of the carbon precursor [47] all play a role. We conclude that the synthesis of $LiFePO_4$/C composites is complex, but have introduced a low-cost and simple CTR method to synthesize $LiFePO_4$/C composites in this study.

The carbon content was determined by total organic carbon (TOC) analysis. The carbon contents of the CTR-$LiFePO_4$/C composites synthesized at 873, 973, and 1073 K were 4.21, 4.46, and 4.52 wt.%, respectively. The higher sintering temperature leads to more residual carbon content due to the complete pyrolysis of PEG at higher temperatures.

Table 2
I_D/I_G ratio, carbon content, and electronic conductivity of the $LiFePO_4$/C composites synthesized at different temperatures.

Temperature (K)	Wavenumber (cm^{-1})		Area (a.u.)	A_D/A_G	A_{sp^3}/A_{sp^2}	Carbon content (%)	Electrical conductivity ($S\,cm^{-1}$)
873	sp^2	1341 (D band)	126781	3.87	0.88	4.21	3.44×10^{-5}
		1592 (G band)	32770				
	sp^3	1150	100543	–			
		1528	39913				
973	sp^2	1346 (D band)	228949	2.94	0.50	4.46	4.42×10^{-4}
		1593 (G band)	77990				
	sp^3	1197	81484	–			
		1519	72001				
1073	sp^2	1354 (D band)	360658	2.65	0.46	4.52	9.14×10^{-5}
		1592 (G band)	135907				
	sp^3	1253	129002	–			
		1520	98082				

3.6. Electrochemical properties

The discharge capacity of the CTR-$LiFePO_4$/C composites synthesized at 873–1073 K at a 0.2*C*-rate between 4.0 and 2.8 V is shown in Fig. 8. The first discharge capacities of the CTR-$LiFePO_4$/C composites synthesized at 873, 923, 973, 1023, and 1073 K were 77, 141, 150, 142, and 132 mAh g^{-1}, respectively. It has been suggested that a too low sintering temperature might lead to poorly crystalline $LiFePO_4$/C, while a too high temperature might result in larger particle sizes. Thus, finding an optimum sintering temperature for $LiFePO_4$/C is the key. The $LiFePO_4$/C treated at 973 K exhibited the best discharge capacity because it had the highest electronic conductivity (4.42×10^{-4} S cm^{-1}, see Table 2), in contrast to the discharge capacity of the sample synthesized at 873 K, which was much lower than the ones synthesized at other temperatures. Evidently, 873 K is probably not high enough to prepare well-crystallized $LiFePO_4$/C and graphene clusters in the carbon coating layer, which is consistent with XRD results. However, the conductivities listed in Table 2 are not intrinsic $LiFePO_4$ conductivities, but conductivities of the $LiFePO_4$/C composites. The measured values were a function of many factors, such as carbon content, distribution, and its structure. Indeed, based on our previous studies, a lower I_D/I_G ratio [48], thinner thickness and more uniform of carbon coating [45], smaller particle size [11], and higher surface area [47] of $LiFePO_4$/C composites were the keys to excellent electronic conductivity and discharge capacity. All of the above might be achieved by choosing carbon sources, using a suitable process, applying a technique of ball milling, controlling calcination temperature, and optimizing the particle size and surface of the carbon precursors.

Fig. 9 shows the discharge capacity of the CTR-$LiFePO_4$/C samples synthesized at 973 K using different amounts of PEG as carbon sources. If carbon content is sufficient for the formation of a thin and uniform conductive layer, it has an effect on discharge capacity. From these figures, it is clear that the CTR-$LiFePO_4$/C composite treated with 80 wt.% PEG exhibited the best discharge performance, while at 70 wt.% PEG, the discharge capacity increased several cycles earlier because the electrolyte slowly penetrated the porous carbon structure on the $LiFePO_4$/C surfaces and reacted with the electrode materials. For example, the discharge capacity of the sample synthesized at 1073 K rose from 137 to 141 mAh g^{-1} after 30 cycles. In addition, the volume change during lithium insertion and extraction may lead to cracking of the carbon layer, which promotes further penetration of the electrolyte [49,50].

The rate performance of the CTR-$LiFePO_4$/C composite between 4.6 and 2.0 V is shown in Fig. 10. It is obvious that the CTR-$LiFePO_4$/C composite showed excellent rate performance due to the presence of PEG, which could carbonize to form well-carbon-networked $LiFePO_4$, as confirmed in the TEM images. The CTR-sample treated with PEG could sustain a 30*C*-rate between 4.6 and 2.0 V due to substantially improved electronic conductivity, and this rate capability is equivalent to charge or discharge in 2 min. These findings further support the viability of this CTR-$LiFePO_4$/C composite for large lithium ion battery application.

3.7. Cyclic voltammetry

Cyclic voltammetry (CV) was carried out to identify the characteristics of the redox reactions in Li-ion cells. The cyclic voltammograms of the CTR-$LiFePO_4$/C composite synthesized with

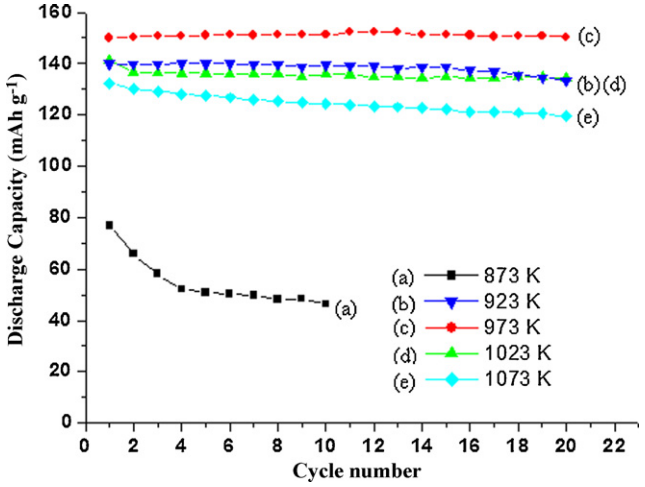

Fig. 8. Discharge capacities of the CTR-$LiFePO_4$/C composites synthesized at (a) 873 K; (b) 923 K; (c) 973 K; (d) 1023 K; (e) 1073 K (0.2*C*, 4.0–2.8 V).

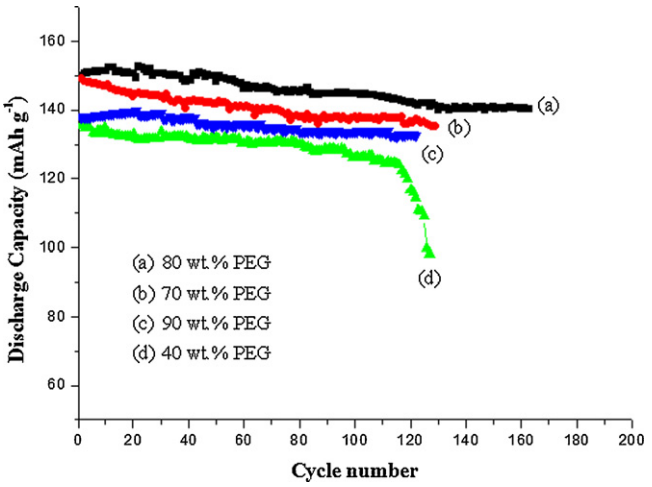

Fig. 9. Discharge capacities of the CTR-$LiFePO_4$/C composites synthesized with (a) 80 wt.%; (b) 70 wt.%; (c) 90 wt.%; (d) 40 wt.% PEG (0.2*C*, 4.0–2.8 V).

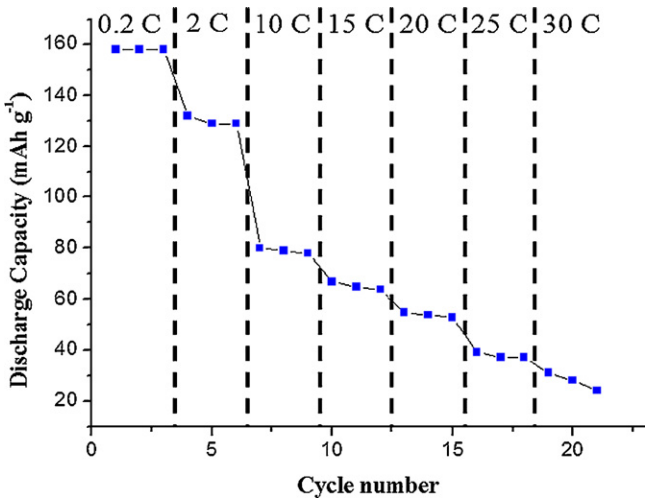

Fig. 10. Rate capability of the $LiFePO_4$/C sample synthesized by the CTR method between 4.6 and 2.0 V.

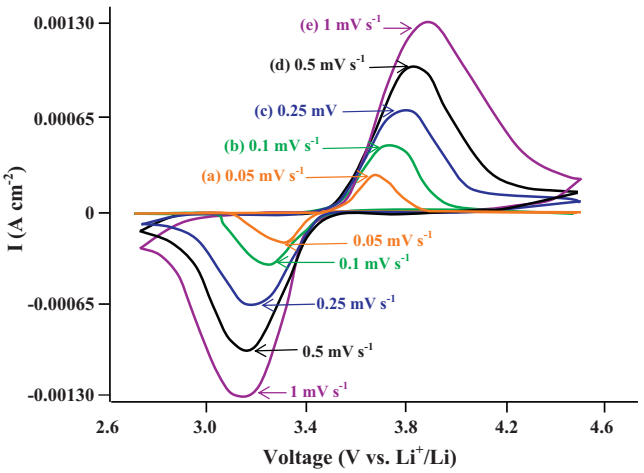

Fig. 12. Cycle voltammograms of CTR-$LiFePO_4$/C electrodes between 2.7 and 4.5 V at different scanning rates: (a) 0.05 mV s^{-1}; (b) 0.1 mV s^{-1}; (c) 0.25 mV s^{-1}; (d) 0.5 mV s^{-1}; (e) 1.0 mV s^{-1}.

80 wt.% PEG are shown in Fig. 11. Only a pair of anodic and cathodic peaks was observed due to the Fe^{2+}/Fe^{3+} redox reaction accompanying Li^+ insertion and extraction [47]. The anodic peak at ~3.55 V represents the oxidation of Fe^{2+} to Fe^{3+}, while the cathodic peak at ~3.30 V is due to the reduction of Fe^{3+} to Fe^{2+}.

The symmetrical sharp redox peaks imply that kinetics of the lithium diffusion is fast in the $LiFePO_4$ structure with better reversibility for lithium intercalation/deintercalation. After five and ten cycles, the redox peaks are sharper than at first cycle, demonstrating less ohmic polarization, because the electrolyte slowly penetrated into the porous carbon structure of the $LiFePO_4$/C composite. These results are consistent with the charge/discharge test shown in Fig. 9.

Fig. 12 shows the cyclic voltammograms of the CTR-$LiFePO_4$/C sample at different scanning rates. The CV peak currents, I_p, during anodic scans are used to evaluate the Li^+ diffusion coefficient D, applying the following equation [51]:

$$I_p = 0.4463 \times F^{3/2} \times S \times n^{3/2} \times C_{Li} \times R^{-1/2} \times T^{1/2} \times D^{1/2} \times v^{1/2}$$

where F is the Faraday constant, S is the electrode area (cm^2), n is the charge transfer number (1 in our case), C_{Li} is the Li-ion concentration in $LiFePO_4$ (mol cm^{-3}), R is the gas constant, T is the absolute temperature (K), v is the potential scan rate (V s^{-1}), I_p is in units of amperes, and D is in units of cm^2 s^{-1}. The scan rates used to calculate D are 0.05, 1, 0.25, 0.5, and 1 mV s^{-1}, and the peak current (I_p) shows a linear relationship with square root of the scan rates ($v^{1/2}$), indicating a diffusion-controlled process, as shown in Fig. 13. Using the above equation, the Li^+ diffusion coefficient of the CTR-$LiFePO_4$/C composite is 2.4×10^{-12} cm^2 s^{-1}, which is two orders of magnitude larger than bare $LiFePO_4$ (~10^{-14} cm^2 s^{-1}). However, if the liquid electrolyte penetrates into the film of $LiFePO_4$/C composites, the D value is overestimated [52].

3.8. Magnetic susceptibility measurements

AC magnetic susceptibility measures the magnetic response of the compound to the ac driving magnetic field. It is known to be a very sensitive means in detecting magnetic phases that appear in the compound. The temperature profile of the in-phase component χ' of the ac magnetic susceptibility of the compound synthesized employing the CTR method is shown in Fig. 14. These data were taken using a weak driving field with a root-mean-square strength of 1 Oe and a frequency of 1000 Hz. The most pronounced feature seen in the $\chi'(T)$ curve of the CTR-sample is the peak at 52 K, reflecting the existence of antiferromagnetic correlations at low temperatures, presumably originated from the magnetic ordering of the Fe ions [53]. The high temperatures portion of this $\chi'(T)$ curve can be described reasonably well by a Curie–Weiss curve (solid

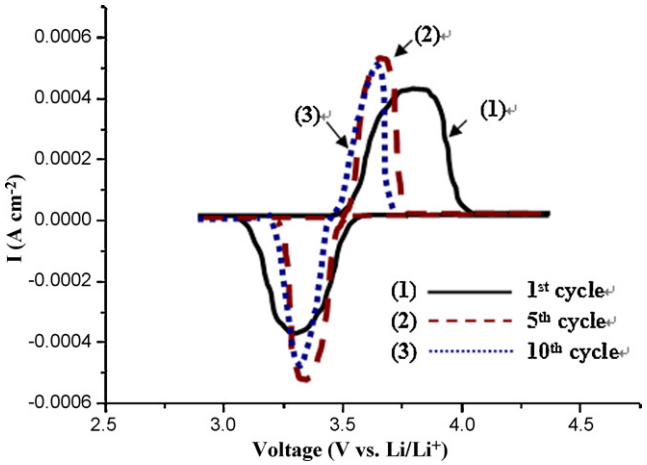

Fig. 11. Cyclic voltammograms of the CTR-$LiFePO_4$/C composite.

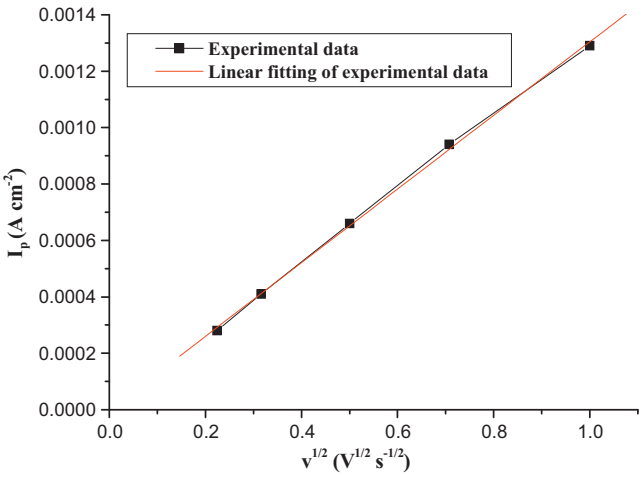

Fig. 13. The plot of the peak current versus square root of scanning rate.

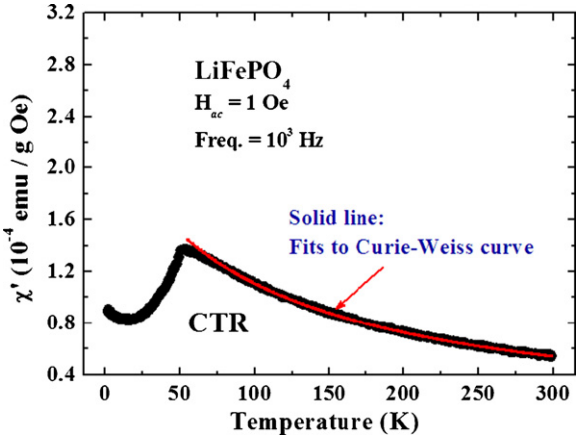

Fig. 14. Temperature profile of the in-phase component of the ac magnetic susceptibility of the compound synthesized employing the CTR method.

line), showing that there is primary one magnetic component in the CTR-sample. It has been reported that the $LiFePO_4$/C composites prepared by the CTR method were more beneficial for long-term application than those prepared by the sol–gel method [54].

4. Conclusions

Olivine $LiFePO_4$/C had been synthesized successfully at different sintering temperatures via a carbothermal reduction method using PEG as a carbon source and reducing agent. In the heating process, PEG led to the formation of a complete carbon network, which improved the electronic conductivity of $LiFePO_4$/C to 4.42×10^{-4} S cm^{-1}. The $LiFePO_4$/C synthesized at 573 K and subsequently at 973 K exhibited excellent electrochemical performance. The charge/discharge tests show that its initial discharge capacity is 150 mAh g^{-1} at a 0.2*C*-rate between 4.0 and 2.8 V. Most of all, the CTR-sample could sustain a 30*C*-rate between 4.6 and 2.0 V. In this study, we developed a low-cost method to synthesize $LiFePO_4$/C composites with the potential for commercialization.

References

[1] A.K. Padhi, K.S. Nanjundaswamy, J.B. Goodenough, J. Electrochem. Soc. 144 (1994) 1188.
[2] A.S. Andersson, J.O. Thomas, J. Power Sources 97–98 (2001) 498.
[3] S. Scaccia, M. Carewska, P. Wisniewski, P.P. Prosini, Mater. Res. Bull. 38 (2003) 1155.
[4] Z. Chen, J.R. Dahn, J. Electrochem. Soc. 149 (2002) A1184.
[5] C.H. Mi, X.B. Zhao, G.S. Cao, J.P. Tu, J. Electrochem. Soc. 152 (2005) A483.
[6] S.Y. Chung, J.T. Bloking, Y.M. Chiang, Nature 1 (2002) 123.
[7] Y.N. Xu, S.Y. Chung, J.T. Bloking, Y.M. Chiang, W.Y. Ching, Electrochem. Solid-State Lett. 7 (2004) A131.
[8] P.S. Herle, B. Ellis, N. Coombs, Nat. Mater. 3 (2004) 147.
[9] Y.D. Cho, G.T.K. Fey, H.M. Kao, J. Solid State Electrochem. 12 (2008) 815.
[10] D. Choi, P.N. Kumta, J. Power Sources 163 (2007) 1064.
[11] G.T.K. Fey, Y.G. Chen, H.M. Kao, J. Power Sources 189 (2009) 169.
[12] N. Ravet, J.B. Goodenough, S. Besner, M. Simoneau, P. Hovington, M. Armand, Proceedings of the 196th ECS Meeting, Hawaii, October 17–22, 1999.
[13] H. Huang, S.C. Yin, L.F. Nazarz, Electrochem. Solid-State Lett. 4 (2001) A170.
[14] G.T.K. Fey, T.L. Lu, J. Power Sources 178 (2008) 807.
[15] F. Croce, A.D. Epifanio, J. Hassoun, A. Deptula, T. Olczac, B. Scrosatia, Electrochem. Solid-State Lett. 5 (2002) A47.
[16] B. Kang, G. Ceder, Nature 458 (2009) 190.
[17] J. Barker, M.Y. Saidi, J.L. Swoyer, Electrochem. Solid-State Lett. 6 (2003) A53.
[18] Y.H. Nien, J.R. Carey, J.S. Chen, J. Power Sources 193 (2009) 822.
[19] N.J. Yun, H.W. Ha, K.H. Jeong, H.Y. Park, K. Kim, J. Power Sources 160 (2006) 1361.
[20] G.X. Wang, L. Yang, Y. Chen, J.Z. Wang, S. Bewlay, H.K. Liu, Electrochim. Acta 50 (2005) 4649.
[21] Y.H. Huang, J.B. Goodenough, Chem. Mater. 20 (2008) 7237.
[22] L.N. Wang, Z.G. Zhang, K.L. Zhang, J. Power Sources 167 (2007) 200.
[23] H.M. Xie, R.S. Wang, J.R. Ying, L.Y. Zhang, A.F. Jalbout, H.Y. Yu, G.L. Yang, X.M. Pan, Z.M. Su, Adv. Mater. 18 (2006) 2609.
[24] M.L. Yuan, X.M. Deng, Eur. Polym. J. 37 (2001) 1907.
[25] S. Tajimi, Y. Ikeda, K. Uematsu, K. Toda, M. Sato, Solid State Ionics 175 (2004) 287.
[26] Z. Xu, L. Xu, Q. Lai, X. Ji, Mater. Res. Bull. 42 (2007) 883.
[27] H. Liu, D. Tang, Solid State Ionics 179 (2008) 1897.
[28] P.P. Prosini, M. Carewska, S. Scaccia, P. Wisniewski, S. Passerini, M. Pasquali, J. Electrochem. Soc. 149 (2002) 886.
[29] H. Liu, J. Xie, K. Wang, J. Alloys Compd. 459 (2008) 521.
[30] X. Zhi, G. Liang, L. Wang, X. Ou, J. Zhang, J. Cui, J. Power Sources 189 (2009) 779.
[31] L. Wang, G.C. Liang, X.Q. Ou, X.K. Zhi, J.P. Zhang, J.Y. Cui, J. Power Sources 189 (2009) 423.
[32] S.J. Kwon, C.W. Kim, W.T. Jeong, K.S. Lee, J. Power Sources 137 (2004) 93.
[33] K.F. Hsu, S.Y. Tsay, B.J. Hwang, J. Power Sources 146 (2005) 529.
[34] B.D. Cullity, S.R. Stock, Elements of X-Ray Diffraction, 3rd ed., Prentice Hall Publishers, New Jersey, USA, 2001 (Chapter 5.2).
[35] J.K. Kim, G. Cheruvally, J.W. Choi, J.U. Kim, J.H. Ahn, G.B. Chob, K.W. Kim, H.J. Ahn, J. Power Sources 166 (2007) 211.
[36] Y.Z. Dong, Y.M. Zhao, Y.H. Chen, Z.F. He, Q. Kuang, Mater. Chem. Phys. 115 (2009) 245.
[37] H. Liu, C. Li, H.P. Zhang, L.J. Fu, Y.P. Wu, H.Q. Wu, J. Power Sources 159 (2006) 717.
[38] A. Yamada, S.C. Chung, K. Hinokuma, J. Electrochem. Soc. 148 (2001) A224.
[39] P. Barpanda, N. Recham, J.N. Chotard, K. Djellab, W. Walker, M. Armanda, J.M. Tarascon, J. Mater. Chem. 20 (2010) 1609.
[40] W.S. Yoon, K.Y. Chung, J. McBreen, K. Zaghib, X.Q. Yang, Electrochem. Solid-State Lett. 9 (2006) A415.
[41] C. Delacourt, P. Poizot, J.M. Tarascon, C. Masquelier, Nat. Mater. 4 (2005) 254.
[42] Z. Zhang, D. Fouchard, J.R. Rea, J. Power Sources 70 (1998) 16.
[43] M.M. Doeff, Y. Hu, F. McLarnon, R. Kostecki, Electrochem. Solid-State Lett. 6 (2003) A207.
[44] Y. Hu, M.M. Doeff, R. Kostecki, R. Finones, J. Electrochem. Soc. 151 (2004) A1279.
[45] Y.D. Cho, G.T.K. Fey, H.M. Kao, J. Power Sources 189 (2009) 256.
[46] J.M. Chen, C.H. Hsu, Y.R. Lin, M.H. Hsiao, G.T.K. Fey, J. Power Sources 184 (2008) 498.
[47] G.T.K. Fey, T.L. Lu, F.Y. Wu, J. Solid State Electrochem. 12 (2008) 825.
[48] C.Z. Lu, G.T.K. Fey, H.M. Kao, J. Power Sources 189 (2009) 155.
[49] S.T. Myung, S. Komaba, N. Hirosaki, H. Yashiro, N. Kumagai, Electrochim. Acta 49 (2004) 4213.
[50] R. Dominko, J.M. Goupil, M. Bele, M. Gaberscek, M. Remskar, D. Hanzel, J. Jamnik, J. Electrochem. Soc. 152 (2005) A858.
[51] D.Y.W. Yu, C. Fietzek, W. Weydanz, K. Donoue, T. Inoue, H. Kurokaw, S. Fujitania, J. Electrochem. Soc. 154 (2007) A253.
[52] J. Xie, N. Imanishi, T. Zhang, A. Hirano, Y. Takeda, O. Yamamoto, Electrochim. Acta 54 (2009) 4631.
[53] R.P. Santoro, R.E. Newnham, Acta Crystallogr. 22 (1967) 344.
[54] A. Ait-Salah, K. Zaghib, A. Mauger, F. Gendron, C.M. Julien, Phys. Stat. Sol. 203 (2006) R1.